NANO LETTERS

2009
Vol. 9, No. 1
12-17

Scanning Tunneling Microscopy of DNA-Wrapped Carbon Nanotubes

Dzmitry A. Yarotski,*,† Svetlana V. Kilina,†,‡ A. Alec Talin,†,§ Sergei Tretiak,†,‡ Oleg V. Prezhdo,|| Alexander V. Balatsky,†,‡ and Antoinette J. Taylor†

Center for Integrated Nanotechnologies, Los Alamos National Laboratory, Los Alamos, New Mexico 87545, Theoretical Division, Los Alamos National Laboratory, Los Alamos, New Mexico 87545, Sandia National Laboratory, Livermore, California 94550, and Department of Chemistry, University of Washington, Seattle, Washington 98195-1700

Received May 21, 2008; Revised Manuscript Received November 24, 2008

ABSTRACT

We employ scanning tunneling microscopy (STM) to reveal the structure of DNA−carbon nanotube complexes with unprecedented spatial resolution and compare our experimental results to molecular dynamics simulations. STM images show strands of DNA wrapping around (6,5) nanotubes at ∼63° angle with a coiling period of 3.3 nm, in agreement with the theoretical predictions. In addition, we observe width modulations along the DNA molecule itself with characteristic lengths of 1.9 and 2.5 nm, which remain unexplained. In our modeling we use a helical coordinate system, which naturally accounts for tube chirality along with an orbital charge density distribution and allows us to simulate this hybrid system with the optimal π-interaction between DNA bases and the nanotube. Our results provide novel insight into the self-assembling mechanisms of nanotube−DNA hybrids and can be used to guide the development of novel DNA-based nanotube separation and self-assembly methods, as well as drug delivery and cancer therapy techniques.

In the past decade, carbon nanotubes (CNT) have been acknowledged as one of the most promising building blocks for future nanoelectronic devices.[1,2] However, practical implementation of CNT-based circuits has long been prevented by the absence of reliable methods to separate CNTs according to their electronic structure and diameter.[1] Moreover, as-prepared solutions usually contain bundles of nanotubes with binding energy of ∼500 eV/m,[1] thus requiring unbundling techniques to be developed in parallel with separation processes.

Recently, several groups reported successful separation of metallic from semiconducting nanotubes based on difference in their physico/chemical properties.[3,4] In addition, O'Connell et al. were able to promote nanotube unbundling through formation of surfactant micelles which permanently encapsulates single CNTs and prevents subsequent rebundling.[5] An alternative approach was demonstrated by Zheng's group, who used single-stranded DNA (ssDNA) binding to the CNTs to simultaneously unbundle and separate CNTs by their electronic properties.[6,7] This simplicity and unsurpassed efficiency of DNA-driven separation has provided new means to study previously unaccessible processes in single nanotubes, such as phonon dynamics[8] and effects of finite CNT length on the spectrum of vibrational excitations.[9] In addition, the unveiled sensitivity of DNA−CNT hybrids electronic and optical response to the molecules bound to DNA has instigated extensive work on sensing applications of such structures.[10−15] Finally, the combination of CNT's unique transport and optical properties along with chemical functionalization with DNA promises a broad range of applications in medicine, drug delivery, and cancer therapy.[16]

Despite significant progress in the practical exploitation of the unique features of DNA−CNT hybrids, very little is presently known about their detailed structure and ensuing electronic properties. Experimental studies demonstrate, for example, that separation outcome is sequence dependent.[6,7] On the other hand, extensive simulations predict a large variation of the possible DNA binding geometries as the DNA sequence changes,[17] ranging from linear DNA alignment along the CNT[18] to wrapping of DNA around the CNT,[19,20] with a finite probability of the DNA insertion into the interior volume of the CNT.[21] These results clearly indicate that certain correlations exist between the efficiency of the separation process and the final hybrid structure. The origin of these correlations should be understood to achieve predictable separation of various types of nanotubes and to further optimize existing procedures.

* Corresponding author, dzmitry@lanl.gov.
† Center for Integrated Nanotechnologies, Los Alamos National Laboratory.
‡ Theoretical Division, Los Alamos National Laboratory.
§ Sandia National Laboratory.
|| Department of Chemistry, University of Washington.

10.1021/nl801455t CCC: $40.75
Published on Web 12/16/2008

Unfortunately, most attempts to determine the mechanisms of the DNA−CNT interaction relied on instrumentation inadequate for the task. For example, conformational changes of DNA on the CNT surface were observed using optical spectroscopy which lacks the resolution necessary to separate responses from closely spaced hybrids and provides information averaged over many different geometries.[11] Even atomic force microscopy (AFM) probes were not able to clearly distinguish various DNA−CNT arrangements, due to inadequate spatial resolution.[6,7] The only instrument capable of simultaneous structural and electronic characterization with subnanometer resolution—scanning tunneling microscopy (STM)—was applied just once to study DNA insertion into the nanotube,[22] and no attempts have been made to characterize other binding geometries of the DNA−CNT system.

Here, we report on the first topographic images of the CNT−DNA hybrids with significant morphological detail. Application of STM allows the direct observation of DNA wrapping around a single CNT with a coiling period of 3.3 nm. Subsequent molecular dynamics (MD) simulations also result in a DNA coiling geometry, and yield a period of 3.2 nm for (6,5) CNT, in excellent agreement with experiment. In addition, we observe the width modulations of the DNA molecule with characteristic lengths of 1.9 and 2.5 nm. These modulations cannot be deduced from the normal binding geometries of DNA nucleotides and CNT, where π-stacking interactions tend to align the nucleotide molecular plane parallel to the tube surface, and further investigations are required to determine their origin. Our results demonstrate the feasibility of CNT−DNA geometry studies with subnanometer resolution and pave the way toward complete characterization of the hybrid structural and electronic properties as a function of DNA sequence.

To form DNA-based nanotube suspensions, a 20-mer DNA sequence of 5′NH_2(C-6)GAGAAGAGAGCAGAAGGAGA-3′ is diluted to approximately 5 mg/mL in phosphate buffer solution with pH 7.4 (PBS 7.4). One milligram of SWCNT from SES Research is dissolved in approximately 250 μL with the DNA solution and then diluted to approximately 0.75 mL with PBS 7.4. The resulting mixture is sonicated at 0 °C for at least 90 min and then centrifuged at 14000 rpm for 90 min. A 0.5 mL portion of the DNA/SWCNT solution is decanted and purified over a NAP-10 column using deionized water as the buffer, with only the first half of the eluted volume being collected. The filtered solution is finally passed again through the NAP-10 column with deionized water as eluent. Raman spectra of thus prepared solution contain six major RBM bands, which are attributed to (13,0), (10,4), (9,3), (9,2), (6,5), and (10,5) tubes.[23] After Raman characterization, a small drop of the DNA−CNT solution is deposited onto p-doped Si(110) substrate and allowed to dry. The samples are then transferred into the STM vacuum chamber and are annealed at 550 °C for 30 min in order to remove the organic residue and the freshly formed oxide layer from the surface. Even though CNT−DNA hybrids in aqueous solution are unstable above 80 °C, the critical temperature for the same constructs adsorbed onto the Si(110) surface appears to be much higher. A commercial

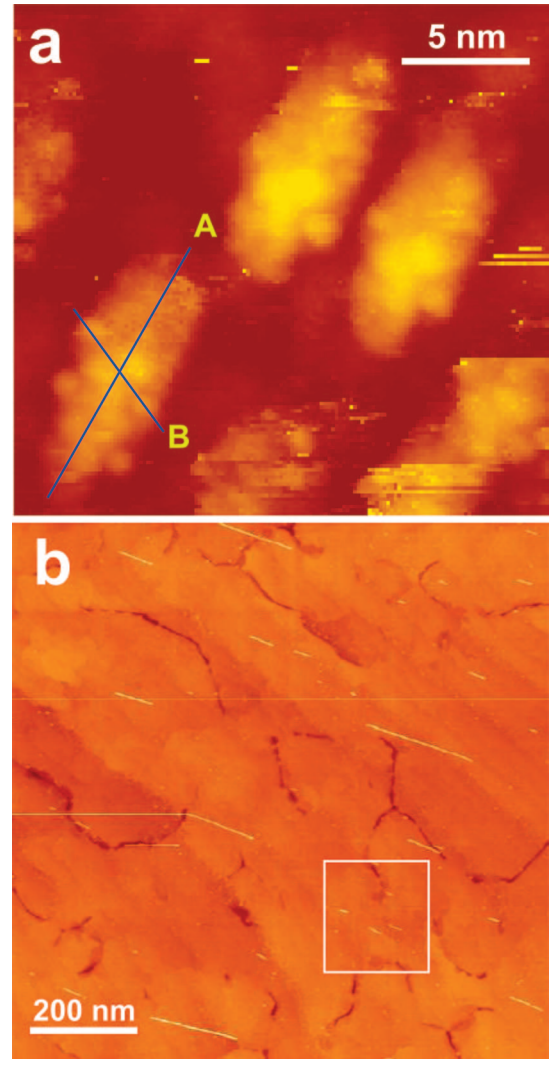

Figure 1. (a) 21 × 21 nm STM topographic image of CNT−DNA hybrids on Si(110) substrate acquired at $I_t = 10$ pA, $U_b = 3$ V; (b) 1 × 1 μm AFM image of the same CNT solution deposited onto Au(111) substrate.

ultrahigh vacuum low-temperature STM system (RHK Technology Inc., UHV300) was used to obtain the topographic images of DNA−CNT hybrids. All measurements were performed at a pressure of 2×10^{-10} Torr and a temperature of 50 K.

A characteristic image of the DNA−CNT sample is shown in the top panel of Figure 1a. DNA-covered parts of the nanotube are visible as large island-like protrusions on a flat substrate surface. Two notable features of the samples are evident in Figure 1a. First, all observed islands have similar structure. This suggests that either we are able to resolve the structure of only one type of CNT−DNA hybrids or hybrids consisting of different CNT types have the same geometry. However, the latter assumption contradicts previous modeling results which demonstrated strong dependence of the DNA wrapping geometry on the CNT chirality.[7,20,24,25] Second, there are no uncovered ends of CNTs visible in the image as one might expect considering the length differences between a typical CNT (~100s of nm) and 20-mer ssDNA. This discrepancy can be explained by the sonication step in

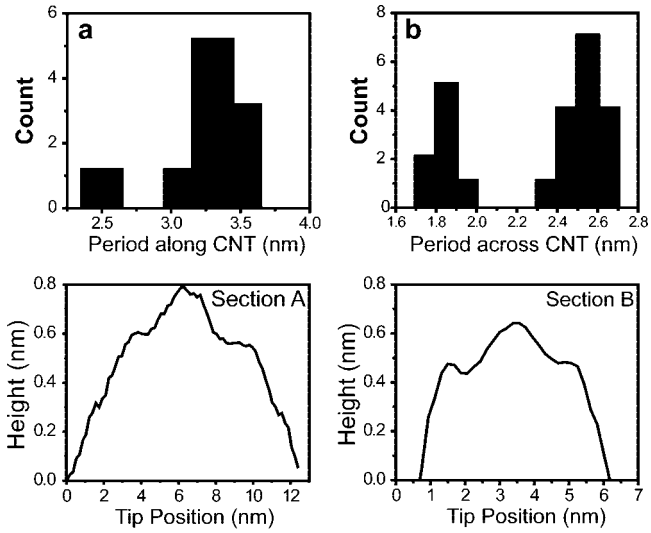

Figure 2. Top panel: Statistical distribution of characteristic lengths of periodic modulations extracted from height profiles along the line A (a) and B (b) in Figure 1a. Bottom panel: Corresponding height profiles.

the sample preparation procedure. Previously, it was found that thorough sonication leads to multiple nanotube breakages resulting in significant nanotube length reduction.[7] In our case, DNA-covered segments serve as fortified islands along the nanotube length, causing the breaks to occur at the edges of such regions and leaving only short 10−15 nm fragments of the original CNT for observation. To check this assumption, we acquire AFM images of the same solution deposited onto the gold substrate (Figure 1b). It is apparent from the image that some areas of the sample contain multiple short (10−50 nm) nanotubes aligned in a definite direction. Similar alignment is also observed in the STM image of hybrids (Figure 1a). The most probable explanation for this alignment comes from the final stage of the sample preparation procedure, where a drop of liquid solution is dried by dragging the filtering paper along the substrate surface. In this case, surface tension forces preferential orientation of prolonged objects along the drag direction.

As mentioned before, there are numerous conformations in which DNA can arrange itself on the CNT. The STM image in Figure 1a clearly demonstrates the DNA strand wrapped around the nanotube. Regular height modulations of the DNA-covered segments of the CNTs are also visible in the image. Two sections of the hybrid profile emphasize the periodic nature of these modulations both along the nanotube and across it (sections A and B, respectively, in bottom panels of Figure 2). We attribute the three height peaks in section A to three DNA coils lying on top of the nanotube surface. The modulation depth of 1−2 Å matches the size of the DNA phosphate backbone which protrudes from the CNT surface, while the nucleotides themselves are aligned parallel to the surface of the nanotube and blend with the background profile.[17,20]

Section B represents the CNT−DNA hybrid profile variations in the direction of DNA coiling. This section is oriented at a 63.4° angle with respect to the nanotube axis. This angle should depend strongly on the particular DNA sequence and CNT type, because nucleotides tend to arrange themselves on the nanotube surface in such a way as to minimize tension in the combined DNA−CNT system.[24] We do not address this dependence in detail here; width the CNT−DNA construct is on the order of 5 nm. This value deviates significantly from the expected combined width of the CNT and two DNA strands on its sides, which should be around 2−3 nm, as will be shown below. We believe that DNA detachment from the nanotube sidewalls during annealing causes this discrepancy, increasing the overall hybrid width. Also, the periodicity of the height profile in section B suggests that there are longitudinal DNA strand distortions which cannot be attributed to any predicted binding mechanisms.

To extract more quantitative information about the observed DNA wrapping geometry, we use the following procedure. First, the cross sections along the longitudinal axis of several CNTs analogous to section A in Figure 1a are taken. In this way, peaks in the topography can be attributed to the DNA strand, and dips represent the underlying CNT surface. Fourier transformation of such a section with respect to the longitudinal coordinate provides well-defined peaks in the spatial frequency domain due to the periodic nature of the profile variation. The characteristic length of the topographic height modulation is obtained by inversion of the spatial frequency of the corresponding peak maximum. The same procedure is then used to extract the modulation lengths across the nanotube (e.g., along DNA molecule), as shown by section B in Figure 1a. The dependence of the frequency of occurrence of a particular period on its magnitude for all hybrids in our images is plotted in the top panel of Figure 2. As can be seen in the top panel of Figure 2a, there is a characteristic period of the height variation along the CNT represented by the peak at 3.3 nm. We attribute this period to the DNA coiling around CNT since it matches very closely the visible separation of the height maximums along section A in the bottom panel of Figure 2a. On the other hand, periodic modulations along the DNA length (section B) have two characteristic lengths, 1.9 and 2.5 nm (Figure 2b). Note that only one of these periods occurs on a particular nanotube, which, in conjunction with a well-defined wrapping period along the CNT, leads us to an assumption that these two different values result from variations in DNA−CNT interaction among the CNTs of the same type.

To obtain additional information about the geometrical features of DNA self-assembling on CNTs, we employ force field MD and first principle quantum mechanical calculations, i.e., density functional theory (DFT). Previous molecular modeling [7,20,25] suggests that DNA bases are attached to the CNT surface due to $\pi-\pi$ overlap between base orbitals and orbitals of aromatic rings of a tube, so-called π-stacking. It is also known that the molecular orbitals (MO) of a CNT strongly correlate with tube chirality and are distributed along natural helical (chiral) coordinates of a tube.[26] Hence, π-stacking forces DNA to follow a helical orbital pattern and wrap around CNTs. We use DFT with the localized Gaussian basis set, as implemented in the Gaussian 03 software

package,[27] to establish the relationship between the tube chirality and the wave function distribution along the tube. For this purpose, we considered several chiral and zigzag semiconductor CNTs, (6,5), (9,1), (7,5), and (10,0), of nearly similar diameters (0.75−0.86 nm) and finite length of about 10−12 nm. Unsaturated chemical bonds at the open tube ends are capped with hydrogen atoms to remove midgap states caused by dangling bonds, as described in detail elsewhere.[28] The most commonly used hybrid functional, the Becke 3-parameter hybrid functional (B3LYP) with 20% of the Hartree−Fock exchange, and the 6-31G basis sets are employed. The B3LYP/6-31G calculations have become the standard in modeling the electronic and optical properties of large organic molecules[29] and were recently successfully applied to determine the energies and localization properties of bright and dark excitons in nanotubes.[30] Thus, the B3LYP/6-31G calculations are expected to provide a reasonable physical picture of the wave function distribution along a CNT.

To construct a hybrid system, a single-strand DNA (ssDNA) is wrapped around a tube in accordance with the tube orbital distribution and natural helical coordinates, described by eq 1 and illustrated in Figure 3b. Next, these hybrid configurations are fed to the CHARM force field geometry optimization that provides energetically favorable morphologies of the DNA strand on the nanotube surface. In our calculations, we consider two ssDNA sequences: GAGAAGAGAGCAGAAGGAGA (20-mer) used in our STM experiment, and a homogeneous oligonucleotide with 40 cytosine bases (40C-mer). All geometry optimizations were performed by means of the HyperChem software package[31] using an energy convergence limit of 0.001 kcal/(Å mol). The length of the tube is chosen to be twice longer (20−30 nm) than the average length observed in the experiment to reduce edge effects on the final results.

The DFT analysis of MO of tubes with different chiralities demonstrates that CNT charge density follows the chiral angle—the angle between the tube axis and the chirality vector—for all considered orbitals. The spatial distribution of lowest unoccupied molecular orbitals (LUMOs), plotted for chiral (6,5) CNTs in Figure 3a, emphasizes a well-defined relationship between the orbital density distribution on the tube surface and the natural symmetry of the tube. Thus, the best π-stacking between a CNT and DNA occurs when the orbitals of a DNA base align with the direction of the maximum MO density of a tube. This conclusion agrees with recent results of similar MD calculations of DNA−CNT system structure.[20]

Although it was numerically predicted that short ssDNA strands can adopt a number of helical conformations on a CNT,[7] the well-defined wrapping geometry observed in our experiment (Figure 1a) suggests the existence of a specific stable helical geometry with wrapping period of 3.3 nm. To resolve this discrepancy, we establish the relationship between the orbital charge density distribution on the tube and the wrapping geometry of the CNT−DNA hybrid. The insert in Figure 3b shows a schematic line (blue) along which DNA can be wrapped around the tube (m,n). This line follows the maximums of the orbital wave function on the tube surface and represents the natural helical coordinates of the tube or the optimal π-stacking line.[26] In the cylindrical coordinates, each point (x_i, y_i, z_i) that belongs to this wrapping line satisfies the equations

$$\varphi_i(z) = \frac{z}{R \tan \Theta} \qquad (1)$$
$$x_i(z) = R \cos \Theta$$
$$y_i(z) = R \sin \Theta$$

Here $\phi_i(z)$ is the rotational angle of the ith atom on a tube surface, Θ is the tube chiral angle, and z is the length along the tube axis per unit rotation angle. $R = R_0 + \Delta$ stands for the helix radius, where R_0 is a tube radius, and $\Delta \sim 0.3$ nm is a typical distance between the tube surface and DNA molecules in π-stacking attachment.[24] When $\phi_i = 2\pi$, the period of wrapping becomes $z = 2\pi R \tan \Theta$. Because both the tube radius and the tube chiral angle depend on the type

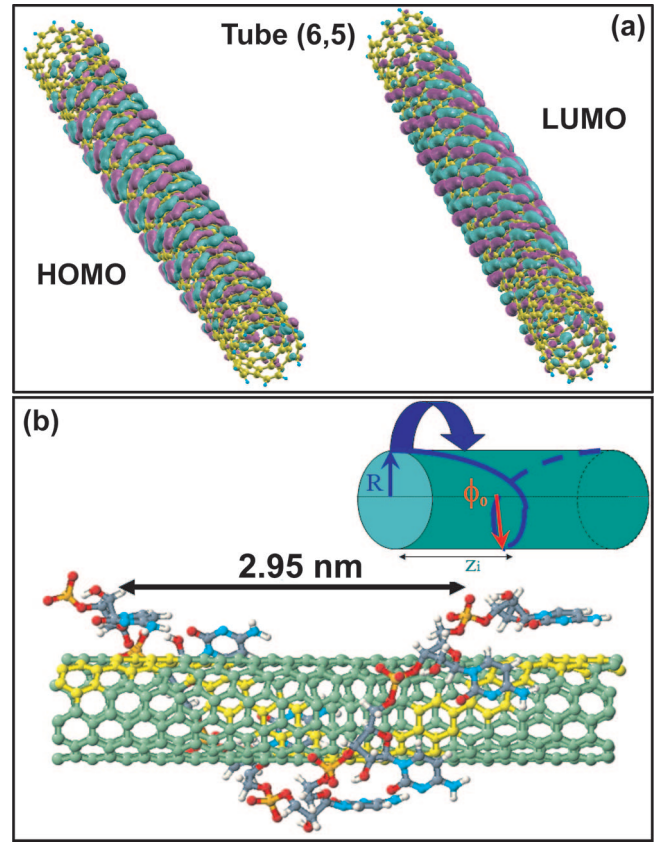

Figure 3. The relation between the orbital charge density distribution of a CNT and the wrapping geometry of a CNT−DNA hybrid. (a) Lowest unoccupied molecular orbitals (LUMO) of the (6,5) tube. The positive or the negative sign of the wave function is shown by the red or blue color, respectively. The orbital charge density is aligned with normal to the tube chiral vector, thus showing a strong orbital charge distribution dependence on natural chiral coordinates of a tube. (b) Schematic representation of DNA wrapping around a CNT (inset) and an initial configuration of the C-oligomer wrapped along the (6,5) tube chirality. Here red, orange, cyan, gray, and white colors represent oxygen, phosphor, nitrogen, carbon, and hydrogen atoms of cytosine, respectively. Green and yellow colors represent carbon atoms of the CNT. Carbon atoms marked by yellow indicate the direction of DNA wrapping with seven cytosine bases per helical turn, which lay parallel to the tube surface and nearly normal to the tube chiral vector, thus increasing $\pi-\pi$ overlap between the base and tube orbitals.

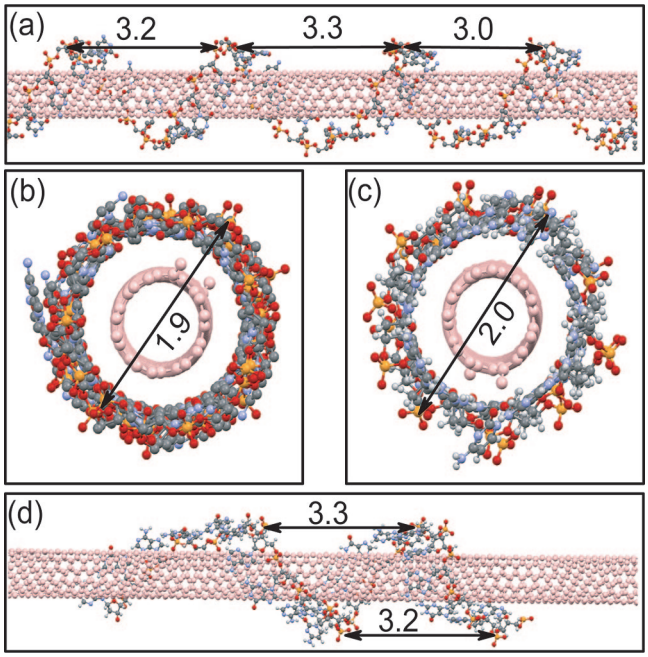

Figure 4. Optimized structures of (6,5) tube wrapped in 40C-oligomer (a, b) and GAGAAGAGAGCAGAAGGAGA-oligomer (c, d). Both structures demonstrate very stable configurations, which do not deviate very much from the initial geometries. DNA bases are positioned almost normally to the tube chiral vector and sugar−phosphate backbone follows the tube chirality. For both DNA wrapping geometries, the average period of DNA helices along the tube is 3.0−3.3 nm, in good agreement with STM images.

of CNT, i.e., indices (*m*,*n*), the wrapping period should also depend on the tube indices (*m*,*n*).

We choose a particular (6,5) tube for subsequent hybrid structure simulations because it provides the best match to the STM imaging results. Indeed, according to the formula for the wrapping period and MD modeling, (6,5) tube ($\Theta \sim 27°$, $R \sim 0.38$ nm) has the wrapping period of $z \sim 3$ nm, matching that observed in the experiments. Moreover, DNA wrapping along the helical orbital pattern of the (6,5) nanotube forms a ∼63° angle with the nanotube axis, which almost exactly reproduces the 63.4° wrapping angle observed with STM. All other nanotube types present in solution have much smaller wrapping periods of 1−1.7 nm and completely different wrapping angles. The short wrapping periods on all the nanotubes except (6,5) result in small gaps, on the order of 0.2−0.8 nm, between the DNA strands. This can explain an observation of a single type of wrapping geometry in STM images, if we assume that our instrument is not able to resolve such closely spaced DNA strands.

First, we consider the CNT−DNA hybrid that consists of the 40C-mer wrapped around the (6,5) tube in accordance with eq 1, as shown in Figure 3b. This configuration is then used to initialize force field geometry optimization which finds the lowest-energy conformation that maximizes the base−nanotube interaction. The final geometry of the (6,5)−40C-mer hybrid is shown in Figure 4, panels a and b. The optimization procedure results in a small geometry deviation from the initial configuration of the hybrid. The helical period along the tube is slightly increased to 3.2 nm, as compared to the initial setting of 2.9 nm. The distance between the tube surface and the aromatic ring of the nucleotide remains ∼0.35 nm, which is typical for π-stacking binding. The tube−phosphor distance is ∼0.47 nm. The average diameter of the (6,5)−40C-mer hybrid, measured as the distance between phosphor atoms laying on the opposite sides of the DNA helix at 1/2 of a helical period from each other, is 1.9 nm. The binding energy between 40C-mer and the (6,5) tube is 0.7 eV per base rationalizing very stable structures of the CNT−DNA hybrid. As expected, hybrids incorporating other types of CNTs, for example (11,10), produce very different helical periods. The (11,10) tube has a chiral angle of 28°, similar to the (6,5) tube, but its diameter is larger (∼1.5 nm). Therefore, eq 1 predicts that the wrapping period of this tube is larger than that for (6,5)−40C-mer hybrid. Indeed, the optimized geometry of the (11,10)−40C-mer hybrid reveals DNA wrapping periods of 4.2 nm with an average hybrid diameter of 2.6 nm. The average separation of the nucleotide carbons from the carbons on the (11,10) tube surface is 0.34 nm and that of the backbone phosphor atoms is ∼0.45 nm. Interestingly, these values are essentially independent of the tube chirality and the DNA sequence. Our simulations for the (9,1) and (7,5) tubes wrapped in 40C-mer, as well as 20-mer ssDNA used in our experiment, show similar tube−phosphor and tube−nucleotide distances of 0.45−0.48 nm and 0.33−0.35 nm, respectively. These data are also very close to the results of recent MD calculations.[20]

Next, we simulate the hybrid constructed from the (6,5) tube and 20-mer DNA used in STM imaging. The initial configuration of the hybrid and the optimization procedure are the same as for CNT−40C-mer described above. The results of simulations are shown in Figure 4, panels c and d. The calculated binding energy of this hybrid is 0.8 eV per base, which is slightly higher than that for (6,5)−40C-mer hybrid. The optimized geometry demonstrates the average DNA wrapping period of 3.2 nm and the hybrid diameter of 2.0 nm. The close match between the simulated DNA wrapping periods for 40C-mer and 20-mer suggests a weak dependence of the DNA wrapping geometry on its chemical structure. On the other hand, the experimental observation of two characteristic periods along the DNA length on the same nanotube points to possible dependence of the DNA wrapping geometry on the factors other than the CNT diameter and chirality, and DNA sequence.

In all considered cases, large binding energies of 0.7−0.8 eV lead to very stable structures of the CNT−DNA hybrids constructed in accordance with the optimal π-stacking conditions (eq 1). The strong interaction between the ssDNA and the CNT might explain the thermal stability of the hybrids, which do not dissociate during 550 °C annealing. The results of our simulations correlate quite well with the binding energies previously measured for the adenine molecules adsorbed on the graphite surface (1 eV),[32] and those obtained from MD[20] and DFT calculations of a single DNA base placed on the (10,0) CNT.[24] We have also checked a few random wrapping geometries of 40C-mer on a (6,5) tube, where the initial position of nucleotides with respect to the

tube surface did not follow the optimal π-stacking line. After optimization these random structures possessed relatively low binding energies (0.1−0.3 eV), leading to a less stable hybrid structure as compared to the ones with the optimal π-stacking along the natural helical tube coordinates.

In conclusion, we have conducted topographic imaging of CNT−DNA hybrid geometry with subnanometer resolution. DNA wrapping around a single CNT was observed with a characteristic coiling period of 3.3 nm, in excellent agreement with the 3.2 nm period predicted by CHARM FF simulations for 20-mer DNA and particular (6,5) CNT chirality. Periodic distortions of 1.9 and 2.6 nm along the DNA strand were also detected on different types of CNTs. At this stage, we are not able to provide plausible explanation for these modulations and will address this effect in future studies. Our molecular modeling unveiled strong correlations between orbital charge density distribution on the tube surface and the wrapping geometry of the CNT−DNA hybrid. These correlations should lead to pronounced dependence of the DNA coiling periods on CNT chirality and diameter and might explain why some DNA sequences work better than others for nanotube separation. Further application of STM to structural and electronic characterization of CNT−DNA hybrids could reveal more details of their formation and provide further guidance for optimization of DNA-assisted carbon nanotubes separation methods through the construction of the most stable DNA−CNT hybrids with the optimal π-staking geometries. Finally, STM studies of electronic signatures of single nucleotides adsorbed onto the carbon nanotube surface should provide comprehensive verification of one of the recently proposed electronic DNA sequencing methods,[24] where distinct resonances in the tunneling spectra of various aminoacids attached to CNT are used for reliable identification of the nucleotide sequence in the DNA strand.

Acknowledgment. We acknowledge support from the Los Alamos National Laboratory LDRD Program. This work was performed, in part, at the Center for Integrated Nanotechnologies, a US Department of Energy, Office of Basic Energy Sciences nanoscale science research center operated jointly by Los Alamos and Sandia National Laboratories. Los Alamos National Laboratory, an affirmative action/equal opportunity employer, is operated by Los Alamos National Security, LLC, for the National Security administration of the US Department of Energy under Contract DE-AC52-06NA25396.

References

(1) *Carbon Nanotubes: Synthesis, Structure, Properties, and Applications*; Dresselhaus, M. S., Dresselhaus, G., Avouris, P., Eds.; Topics in Applied Physics, Vol. 80; Springer-Verlag: Berlin, 2001.
(2) Avouris, P.; Chen, J. *Mater. Today* **2006**, *9*, 46.
(3) Chattopadhyay, D.; Galeska, I.; Papadimitrakopoulos, F. A. *J. Am. Chem. Soc.* **2003**, *125*, 3370.
(4) Krupke, R.; Hennrich, F.; Lohneysen, H. V.; Kappes, M. M. *Science* **2003**, *301*, 344.
(5) O'Connell, M. J.; Bachilo, S. M.; Huffman, C. B.; Moore, V. C.; Strano, M. S.; Haroz, E. H.; Rialon, K. L.; Boul, P. J.; Noon, W. H.; Kittrell, C.; Ma, J.; Hauge, R. H.; Weisman, R. B.; Smalley, R. E. *Science* **2002**, *297*, 593.
(6) Zheng, M.; Jagota, A.; Strano, M. S.; Santos, A. P.; Barone, P.; Chou, S. G.; Diner, B. A.; Dresselhaus, M. S.; Mclean, R. S.; Onoa, G. B.; Samsonidze, G. G.; Semke, E. D.; Usrey, M.; Walls, D. J. *Science* **2003**, *302*, 1545.
(7) Zheng, M.; Jagota, A.; Semke, E. D.; Diner, B. A.; Mclean, R. S.; Lustig, S. R.; Richardson, R. E.; Tassi, N. G. *Nat. Mater.* **2003**, *2*, 338.
(8) Chou, S. G.; Plentz, F.; Jiang, J.; Saito, R.; Nezich, D.; Ribeiro, H. B.; Jorio, A.; Pimenta, M. A.; Samsonidze, Ge. G.; Santos, A. P.; Zheng, M.; Onoa, G. B.; Semke, E. D.; Dresselhaus, G.; Dresselhaus, M. S *Phys. Rev. Lett.* **2005**, *94*, 127402.
(9) Chou, S. G.; Son, H.; Zheng, M.; Saito, R.; Jorio, A.; Dresselhaus, G.; Dresselhaus, M. S. *Chem. Phys. Lett.* **2007**, *443*, 328.
(10) Staii, C.; Johnson, A. T. *Nano Lett.* **2005**, *5*, 1774.
(11) Heller, D. A.; Jeng, E. S.; Yeung, T.-K.; Martinez, B. M.; Moll, A. E.; Gastala, J. B.; Strano, M. S. *Science* **2006**, *311*, 508.
(12) Xu, Y.; Pehrsson, P. E.; Chen, L.; Zhang, R.; Zhao, W. *J. Phys. Chem. C* **2007**, *111*, 8638.
(13) Gui, E.-L.; Li, L.-J.; Lee, P. S.; Lohani, A.; Mhaisalkar, S. G.; Cao, Q.; Kang, S. J.; Rogers, J. A.; Tansil, N. C.; Gao, Z. *Appl. Phys. Lett.* **2006**, *89*, 232104.
(14) Johnson, A. T. C.; Staii, C.; Chen, M.; Khamis, S.; Johnson, R.; Klein, M. L.; Gelperin, A. *Semicond. Sci. Technol.* **2006**, *21*, S17.
(15) Barone, P. W.; Baik, S.; Heller, D. A.; Strano, M. S. *Nat. Mater.* **2005**, *4*, 86.
(16) Kam, N. W. S.; O'Connell, M.; Wisdom, J. A.; Dai, H. J. *Proc. Natl. Acad. Sci. U.S.A.* **2005**, *102*, 11600.
(17) Gao, H.; Kong, Y. *Annu. Rev. Mater. Res.* **2004**, *34*, 123.
(18) Zhao, X.; Johnson, J. K. *J. Am. Chem. Soc.* **2007**, *129*, 10438.
(19) Lu, G.; Maragakis, P.; Kaxiras, E. *Nano Lett.* **2005**, *5*, 897.
(20) Johnson, R. R.; Johnson, A. T. C.; Klein, M. L. *Nano Lett.* **2008**, *8*, 69.
(21) Gao, H.; Kong, Y.; Cui, D.; Ozkan, C. S. *Nano Lett.* **2003**, *3*, 471.
(22) Ijima, M.; Watabe, T.; Ishii, S.; Koshio, A.; Yamaguchi, T.; Bandow, S.; Iijima, S.; Suzuki, K.; Maruyama, Y. *Chem. Phys. Lett.* **2005**, *414*, 520.
(23) Jorio, A.; Saito, R.; Hafner, J. H.; Lieber, C. M.; Hunter, M.; McClure, T.; Dresselhaus, G.; Dresselhaus, M. S. *Phys. Rev. Lett.* **2001**, *86*, 1118.
(24) Meng, S.; Maragakis, P.; Papaloukas, C.; Kaxiras, E. *Nano Lett.* **2007**, *7*, 45.
(25) Lustig, S. R.; Jagota, A.; Khripin, C.; Zheng, M. *J. Phys. Chem. B* **2005**, *109*, 2559.
(26) Kilina, S.; Tretiak, S.; Doorn, S. K.; Luo, Z.; Papadimitrakopoulos, F.; Piryatinski, A.; Saxena, A.; Bishop, A. R. *Proc. Natl. Acad. Sci. U.S.A.* **2008**, *105*, 6797.
(27) Frisch, M. J.; Trucks, G. W.; Schlegel, H. B.; Scuseria, G. E.; Robb, M. A.; Cheeseman, J. R.; Montgomery J. A., Jr.; Vreven, T.; Kudin, K. N.; BurantJ. C.; Millam, J. M.; Iyengar, S. S.; Tomasi, J.; Barone, V.; Mennucci, B.; Cossi, M.; Scalmani, G.; Rega, N.; Petersson, G. A.; Nakatsuji, H.; Hada, M.; Ehara, M.; Toyota, K.; Fukuda, R.; Hasegawa, J.; Ishida, M.; Nakajima, T.; Honda, Y.; Kitao, O.; Nakai, H.; Klene, M.; Li, X.; Knox, J. E.; Hratchian, H. P.; Cross, J. B.; Bakken, V.; Adamo, C.; Jaramillo, J.; Gomperts, R.; Stratmann, R. E.; Yazyev, O.; Austin, A. J.; Cammi, R.; Pomelli, C.; Ochterski, J. W.; Ayala, P. Y.; Morokuma, K.; Voth, G. A.; Salvador, P.; Dannenberg, J. J.; Zakrzewski, V. G.; Dapprich, S.; Daniels, A. D.; Strain, M. C.; Farkas, O.; Malick, D. K.; Rabuck, A. D.; Raghavachari, K.; Foresman, J. B.; Ortiz, J. V.; Cui, Q.; Baboul, A. G.; Clifford, S.; Cioslowski, J.; Stefanov, B. B.; Liu, G.; Liashenko, A.; Piskorz, P.; Komaromi, I.; Martin, R. L.; Fox, D. J.; Keith, T.; Al.Laham, M. A.; Peng, C. Y.; Nanayakkara, A.; Challacombe, M.; Gill, P. M. W.; Johnson, B.; Chen, W.; Wong, M. W.; Gonzalez, C.; Pople, J. A. *Gaussian 03 (Rev. C.02)*: Gaussian Inc.: Wallingford, CT, 2003.
(28) Kilina, S.; Tretiak, S. *Adv. Funct. Mater.* **2007**, *17*, 3405.
(29) Dreuw, A.; Head-Gordon, M. *Chem. Rev.* **2005**, *105*, 4009.
(30) Tretiak, S. *Nano Lett.* **2007**, *7*, 2201.
(31) *HyperChem Lite v. 2*, Hypercube Inc., 1115 NW 4th St., Gainesville, FL 32601, 1991.
(32) Freund, J. Ph. D. *Thesis*, Ludwig-Maximilians University, München, 1998.

NL801455T